JACS
JOURNAL OF THE AMERICAN CHEMICAL SOCIETY

Article

pubs.acs.org/JACS

Sub-Nanosecond Resonance Energy Transfer in the Near-Infrared within Self-Assembled Conjugates of PbS Quantum Dots and Cyanine Dye J-Aggregates

Chen Wang and Emily A. Weiss*

Department of Chemistry, Northwestern University, 2145 Sheridan Road, Evanston, Illinois 60208-3113, United States

Supporting Information

ABSTRACT: Energy transfer (EnT) of near-infrared (NIR) excitons enables applications in harvesting of solar energy and biological imaging. Fast exciton extraction from NIR-absorbing Pb-chalcogenide quantum dots (QDs) may allow utilization of the photon down-conversion (multiple exciton generation) process that occurs in those QDs to amplify signal in QD-based sensors or photocurrent in QD-based photovoltaics. This paper describes subnanosecond extraction of NIR excitons from PbS QDs by adsorbed J-aggregates of cyanine dye in aqueous dispersions. The QD/J-aggregate complexes form through electrostatic self-assembly, and the rate and yield of EnT within the complexes can be optimized by adjusting spectral overlap between QD emission and the J-aggregate absorption, which are controlled by density of charged ligands on the QD surface and the pH. The primary EnT pathways have rate constants ranging from $(800\ \text{ps})^{-1}$ to $(2.2\ \text{ns})^{-1}$, which are 1−2 orders of magnitude faster than previously reported examples with PbS QDs as exciton donors. The fastest EnT process occurs in 90 ps and is potentially competitive with Auger recombination of biexcitonic states in PbS QDs.

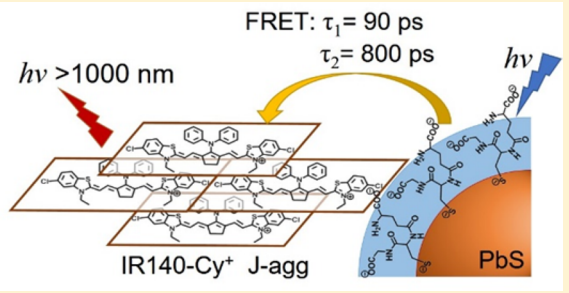

INTRODUCTION

This paper describes the observation of subnanosecond Förster resonance energy transfer (FRET) of near-infrared (NIR, ∼1.2 eV) excitons from PbS quantum dots (QDs) to adsorbed J-aggregates (J-agg) of a cyanine organic dye. Pb-chalcogenide QDs have strong absorption and narrow-line-width, high-quantum-yield emission that span the low-energy portion of the visible spectrum and the NIR spectrum. This spectral coverage is useful in (i) sensitizing photovoltaic[1−3] and photocatalytic devices[4−6] in the portion of the solar spectrum that is not often exploited by organic or semiconductor dyes and (ii) fluorescent tracking of biomolecules *in vivo*.[7,8] A slightly more exotic but potentially very impactful application of PbS QDs is photon downconversion through a process called carrier multiplication,[9,10] which produces multiple charge carriers or multiple NIR photons per photon absorbed and thereby enhances the photocurrent within a photovoltaic device or photodiode or the number of photons emitted by a chemical or biological sensor.[11−13] Utilizing this mechanism requires fast extraction of excitons within the multiexciton states produced by the downconversion process, before they annihilate each other through Auger recombination.[13−15] Subnanosecond extraction of visible-wavelength excitons from cadmium chalcogenide QDs to molecules is fairly routine,[16−19] but extraction of NIR excitons from PbS(Se) QDs by other PbS(Se) QDs through FRET[20−23] or by the triplet states of organic dyes through Dexter energy transfer[24,25] is reported to occur with time constants greater than 10 ns, which is not competitive with Auger recombination (10−200 ps).[13,26,27] Additionally, there are no reports of the use of organic chromophores as FRET acceptors for lead chalcogenide QDs, probably because of the lack of NIR-absorbing dyes and the low emission quantum yields of those that are available.

Here, we demonstrate subnanosecond extraction of NIR excitons from PbS QDs to adsorbed J-agg of a cyanine dye, IR140-Cy$^+$. We prepare the FRET conjugates through self-assembly of positively charged dye molecules on the negatively charged QD surface, which is coated in glutathione (GSH) ligands that solubilize the QD in water[8] and provide a scaffold for electrostatic self-assembly of the conjugates. J-agg, in general, are formed by dye molecules with their transition dipoles coherently coupled in a "head-to-tail" or slip-stacked arrangement. Exciton coupling within J-agg leads to absorption and emission spectra that are bathochromically shifted and narrow with respect to the spectrum of the monomer.[28−30] The narrow and very structure-sensitive absorption of the J-agg allows us to optimize the spectral overlap with the emission of PbS QDs by tuning the surface coverage and protonation state of the GSH ligands.

In the optimized QD/J-agg conjugate, FRET occurs on a subnanosecond time scale, which is 1−2 orders of magnitude faster than any other reported instances of FRET with PbS QDs as energy donors. The fastest energy transfer pathway we observe from QD to a J-agg (with τ = 90 ps) is competitive with typical Auger recombination rates of biexcitons in PbS

Received: April 21, 2016
Published: June 30, 2016

ACS Publications © 2016 American Chemical Society

DOI: 10.1021/jacs.6b04087
J. Am. Chem. Soc. 2016, 138, 9557−9564

QDs and is therefore a means of spatially separating the biexctionic state across two chromophores in order to preserve and use the downconverted excitons to produce photocurrent or photoluminescence.

EXPERIMENTAL METHODS

Synthesis of Oleate-Capped PbS Quantum Dots. We synthesized PbS QDs with a first excitonic absorption that peaks at 900 nm using a protocol adapted from that reported by Hines et al.[31] We dissolved 0.36 g of lead oxide (PbO, Sigma-Aldrich, 99.999%) in 18.95 mL of 1-octadecene (ODE, Sigma-Aldrich, 90%) and 1.05 mL of oleic acid (OA, Sigma-Aldrich, 90%) in a 50 mL three-necked flask at 150 °C under N_2 atmosphere. The solution was kept at 150 °C for 30 min and then cooled to 110 °C. We pulled vacuum (<0.1 Torr) on the flask for 15 min and then returned it to N_2 atmosphere. The sulfur precursor was prepared by adding 0.17 mL of bis(trimethylsilyl)sulfide (TMS, Sigma-Aldrich) to 8 mL of anhydrous ODE, purged with dry N_2 for 1 h at room temperature in a glovebox filled with N_2. We quickly injected the sulfur precursor into the flask containing the lead precursor and carefully maintained the temperature of the reaction mixture at 100 °C. After reacting for 10 min, we quenched the reaction by quickly merging the flask into iced water. We added 100 mL of methanol to the reaction mixture to wash the as-synthesized PbS QDs. The layer with PbS QDs was separated from the mixture by centrifuging at 3500 rpm for 20 min. After removing the supernatant, the QDs were precipitated again by adding 50 mL of acetone and centrifuging at 3500 rpm for 20 min a second time. We redispersed the resulting pellets with a small amount of hexanes, added 50 mL of acetone, centrifuged at 3500 rpm for 20 min a third time, removed the supernatant, dried the QD pellets under N_2 flow, and dispersed the QDs in chloroform.

Ultrafast Transient Absorption Spectroscopy (fs-TA). Details of the ultrafast transient absorption spectroscopy (fs-TA) setup can be found elsewhere.[32] Briefly, fs-TA experiments were conducted with a commercial system (Ultrafast Systems LLC, Helios) powered by a Ti:sapphire amplifier (Spectra-Physics, Solstice). The 800 nm, 2.5 mJ, 100 fs pulse generated by the amplifier was split to form pump and probe beams. The pump beam was directed through an optical parametric amplifier (Light Conversion, TOPAS-C) with sum-frequency generation to produce pump pulses at wavelengths of 470, 930, 980, and 1000 nm. A small portion of the amplifier output was directed through sapphire windows to generate a white-light continuum probe in the visible (3 mm thick plate) or NIR (1.2 cm thick plate) spectral regions. The pump and the probe were focused onto the sample, which was contained in a 2 mm quartz cuvette. During data collection, all samples were stirred continuously.

The instrument response function (IRF) of the TA setup was determined by measuring full width at half-maximum of optical Kerr effect response of CCl_4 in the same quartz cuvette. The IRF was 350 fs for the NIR-probe experiment and 160 fs for the visible-probe experiment.

RESULTS AND DISCUSSION

Preparation of Water-Soluble PbS QDs. Water-soluble PbS QDs were prepared by exchanging the native oleate ligands of the QDs, synthesized as described in the Experimental Methods section, for glutathione through a method adapted from the procedure of Deng et al.[8] GSH was dissolved in water to produce a 10 mM solution, and the pH value of the solution was adjusted to 7.0 by adding KOH. The GSH solution was then diluted to 1 mM, and 5 mL of it was added to 5 mL of 10 μM OA-capped PbS QDs. We shook the mixture for 30 min using a vortex shaker and then separated the organic and aqueous layers by centrifugation at 3500 rpm for 5 min. We repeated the same GSH exchange process four times to produce three different samples with different surface coverages of GSH on the QD: QD-1, which is collected after two rounds of ligand exchange, QD-2, which is collected after three rounds of ligand exchange, and QD-3, which is collected after four rounds of ligand exchange. We purged the resulting aqueous solutions of QDs with N_2 for 1 h and then filtered them using syringe filters with a pore size of $\leq$0.22 μm.

The absorption spectra of the PbS QDs shift to lower energies with increasing coverage of GSH, as is expected for adsorption of ligands that bind through a thiolate.[33−35] The spectrum of the QD-1 sample, which has the lowest surface coverage of GSH, shifts to a lower energy by 10 nm (to 910 nm) from that of the OA-capped QDs. The spectrum of the QD-3 sample, which has the highest coverage of GSH, shifts to a lower energy by 28 nm (to 928 nm) from that of the OA-capped QDs (Figure 1).

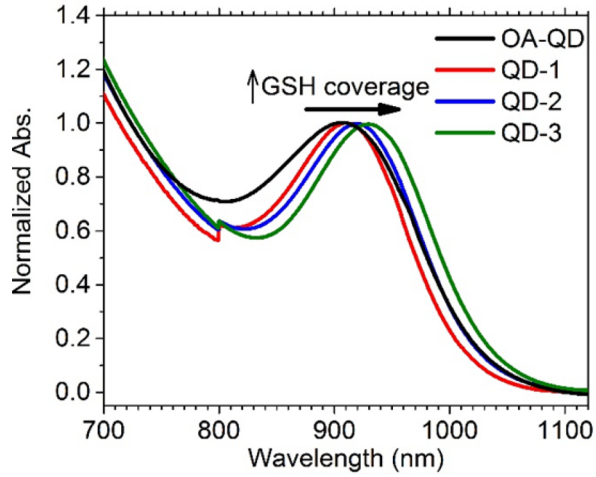

Figure 1. Ground-state absorption spectra of oleate (OA)-capped PbS QDs in $CHCl_3$ (black) and three separately prepared batches of GSH-capped QDs (red, blue, and green) in H_2O, all normalized to the heights of their first excitonic absorptions. A larger bathochromic shift of the absorption spectrum corresponds to a larger surface coverage of GSH, controlled as described in the text. The discontinuity at ~800 nm is due to a grating change in the spectrometer.

Preparation of QD/J-agg Conjugates. We diluted the aqueous dispersions of GSH-capped PbS QDs so that the optical density at the peak of the first excitonic transition was 0.03 cm^{-1}. We adjusted the pH values of the QD dispersions with HCl or KOH and then added a concentrated solution (~550 μM) of IR140-Cy^+ (Sigma-Aldrich) in MeOH to 3 mL of the QDs while stirring vigorously. The samples were sonicated for 2 h before use.

Structure of Adsorbed J-Aggregates Is Controlled by the Surface Charge of the QD. The cyanine dye, IR140-Cy^+, which we will refer to as Cy^+, disperses as a monomer in polar organic solvents such as alcohols; the monomer has an absorption maximum at 800 nm (Figure 2A). Cy^+ is insoluble in water.[36] Directly adding Cy^+ to water or to aqueous solutions of GSH molecules (at the same concentrations and pH values as those used for the GSH-capped QDs mixtures) results in formation of H-aggregates of Cy^+ with absorption bands hypsochromically shifted from those of the monomer (Figure S1). These H-aggregates are unstable in water and precipitate within 1 h. The GSH-capped QDs "solvate" Cy^+ in aqueous solution by formation of complexes of the negatively charged GSH-capped QDs with the positively charged J-agg of the dye (Scheme 1), which has an absorption spectrum that is

DOI: 10.1021/jacs.6b04087
J. Am. Chem. Soc. 2016, 138, 9557−9564

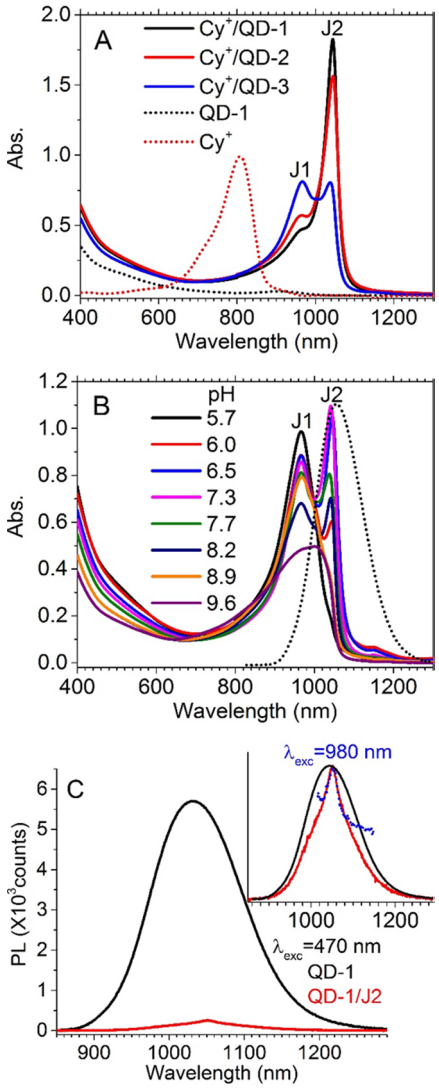

Figure 2. (A) Ground-state absorption spectra (solid lines) of QD/J-agg conjugates formed by mixing 5 μM IR140-Cy$^+$ with three separate batches of GSH-capped PbS QDs (with different coverages of GSH), at pH 7.7. Spectra of QD-1 (without added Cy$^+$) and Cy$^+$ monomer in methanol are plotted in A for comparison. (B) Ground-state absorption spectra (solid lines) of QD/J-agg conjugates formed by mixing 5 μM IR140-Cy$^+$ with PbS QDs from the QD-3 sample at different pH values. The PL spectrum of QD-3 (dotted line) is also plotted to illustrate the spectral overlap with J-agg absorption. (C) PL spectra of QD-1 and QD-1/J2 conjugates (where 70% of Cy$^+$ is in the form of J2 aggregates and 30% is form of J1 aggregates) in aqueous solution. The inset shows the same spectra normalized to their peak maxima, for comparison of the lineshapes. In the inset to C, a PL spectrum of QD-1/J2, acquired by exciting J2 directly at 980 nm, is shown in blue to highlight its overlap with appearance of the emission feature of J2 in the spectrum acquired with 470 nm excitation of the conjugates.

bathochromically shifted from that of the monomer (Figure 2A). The QD/J-agg conjugated systems are soluble for at least 24 h at all pH values above 5.5. On mixing of Cy$^+$ with the QDs, the only Cy$^+$ molecules that remain solvated are those adsorbed to the surfaces of the QDs.

We identify two major types of J-agg, differentiated by their optical spectra. We denote aggregates with an absorption maximum at 965 nm as "J1" and aggregates with an absorption

Scheme 1. One Possible Structure for Self-Assembled Conjugates of IR140-Cy$^+$ J-Aggregates and GSH-Capped PbS QDs

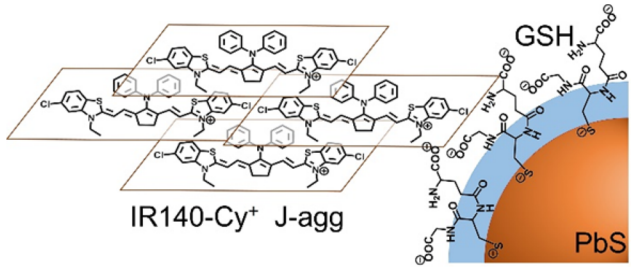

maximum at 1040 nm as "J2" (Figure 2A). The absorption spectrum of J2 resembles that of the J-agg formed with the sulfonate-decorated version of the same cyanine dye (denoted IR140-Cy$^-$).[37] The absorption band of J2 is narrower than that of J1, which implies that J2 is a more ordered aggregate than J1. The large bathochromic shift of the spectra of these J-agg relative to that of the monomer due to exciton coupling leads to spectral overlap between their absorption spectra and emission of the QDs that is not achieved by the monomer. Importantly, the spectral overlap between QD emission and aggregate absorption is much larger for J2 than for J1 (for this QD size), as shown in Figure 2B. Scheme 2 shows a frontier orbital energy diagram of the QDs and Cy$^+$ in its monomer and J-agg forms.

Scheme 2. Frontier Orbital Energy Diagram of the PbS QD and IR140-Cy$^+$ Dye Monomer and the J-Aggregates Formed in This Study[a]

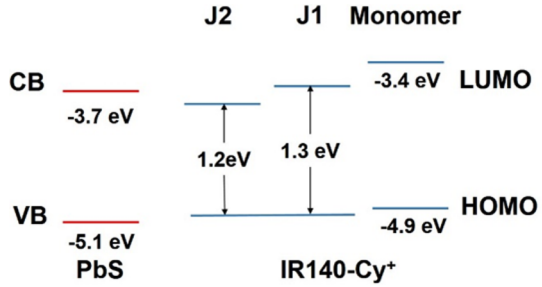

[a]All listed energies are relative to the vacuum level. The valence band (VB)-edge energy of the PbS QDs is measured by ultraviolet photoemission spectroscopy in ref 39, and the conduction band (CB)-edge is the VB-edge plus the optical bandgap. The energy of the HOMO of the IR140-Cy$^+$ monomer was determined by cyclic voltammetry. The energy of the LUMO of the dye equals the HOMO energy plus the excited state energy. The orbital energies of the J-agg are not known precisely, but aggregation of this dye typically causes a slight stabilization of the HOMO.[40] Thus, we assume the HOMO-LUMO gap to equal the energy of the optical absorption of the J-aggregate.

The self-assembly behavior of Cy$^+$ on GSH-QDs is primarily controlled by electrostatic interactions between the negatively charged GSH groups on the QD surface (the density of which is controlled by the ligand exchange procedure and by pH) and the positively charged J-agg, so the amount of J-agg that forms and the relative population of J1 and J2 depends on the surface coverage of GSH ligands and the pH of the solution. The pK_a of the functional groups of GSH ligands that are available to interact with the J-agg are 2.38 (COOH), 3.70 (COOH), and

DOI: 10.1021/jacs.6b04087
J. Am. Chem. Soc. 2016, 138, 9557−9564

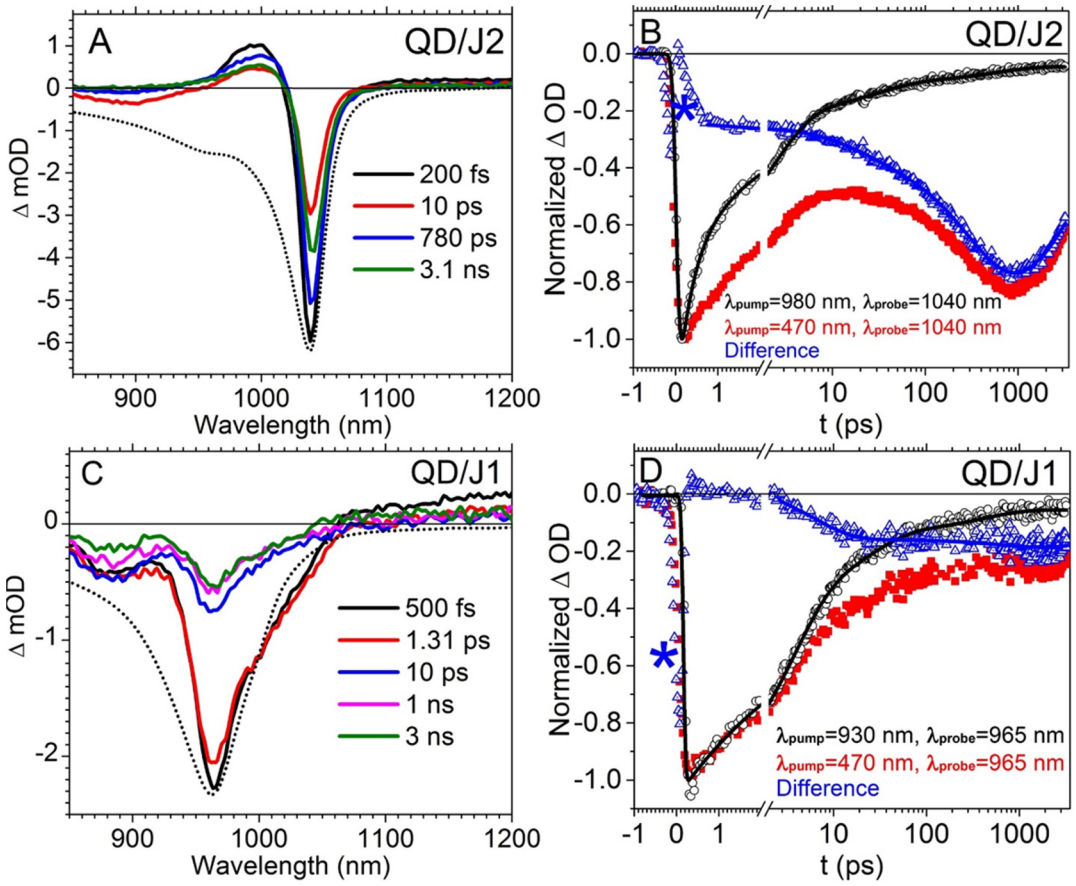

Figure 3. TA spectra (A and C) and normalized TA kinetic traces (B and D) of the QD/J2 and QD/J1 conjugates, as labeled in the legends. (A and C) TA spectra at a series of time delays after >95% selective excitation of the QDs at 470 nm. These spectra consist of the ground state bleach of J2 at 1040 nm and the ground state bleach of J1 at 965 nm, and photoinduced absorptions from J2 and J1 at ∼900−1000 nm. In A, the ground-state bleach of J1 at 965 nm is obscured by the signals from J2. Inverted ground-state absorption spectra of the two conjugates are plotted in A and C as dotted lines to compare with the corresponding TA spectra. (B and D) Normalized kinetic traces extracted at 1040 nm from the TA spectrum of QD/J2 (B), and traces extracted at 965 nm from the spectrum of QD/J1 (D), after pumping the QD at 470 nm. Also shown in black are kinetic traces at the same probe wavelengths but after direct excitation of the J-agg (at 980 nm for J2 or 930 nm for J1). The traces resulting from direct excitation of J-agg are fit with a sum of exponential decays, as detailed in Table S1. The difference between the red and black traces in B and D are plotted in blue and fit with a sum of two exponential growth terms, with or without an exponential decay term as needed. "*" indicates an artifactual growth feature caused by incomplete subtraction of the red and black traces around time zero due to slightly different IRFs of the two experiments. Table 1 lists all fitting parameters for the relevant traces.

8.61 (NH_3^+).[38] The total amount of Cy^+ attached to each QD surface, as measured from the integrated intensity of its absorption band (J1+J2), increases as the pH increases to 7.5 or 8.0 (depending on the synthetic batch of QDs) and then decreases with further increase of pH, probably because in very basic conditions the increasing concentration of the counter-ions K^+ compete with Cy^+ for binding sites. As the GSH coverage increases (from QD-1 to QD-3), the fraction of total aggregates in the J1 form increases (Figure 2A), suggesting that increasing the density of negatively charged binding sites favors the formation of the less-ordered J1-aggregate.

The effect of pH on the formation of J-agg is illustrated in Figure 2B for the QD-3 sample. At pH 5.7, only complexes with J1 form. As the pH increases above 6.0, the absorption of J2 increases until pH 7.7, and then the J2/J1 ratio decreases at higher pH. The sensitive dependence of aggregation on pH suggests that hydrogen bonding in addition to electrostatic interactions may play a role in the assembly. Specifically, changing the pH from 5.5 to 8 should not cause a large change in the number of negatively charged centers on the QD,[38] but could affect the hydrogen bonding interaction between the dye and the solvent molecules, as has been reported for aggregates of carotenoids.[41] We do not completely understand the relationship between pH and dye assembly, but the sensitivity of aggregate structure to pH provides us with a precise way to prepare samples with controlled J1/J2 ratios (Figure 2B). We are unable to obtain complexes with only J2-type aggregates, but we achieve the maximum J2 yield (≥65%) by using the QD-1 sample at pH 7.7.

The absorption spectra of the QD/J-agg conjugates in the 400−550 nm region is enhanced with decreasing pH. In this spectral region, the Cy^+ monomer and aggregates have very low oscillator strength. We therefore conclude that the increased signal in this region is due to scattering by either very large (but soluble) dye aggregates or QD clusters. Agglomeration of the QDs is possibly caused by the lower ζ-potential of the particles upon protonation of GSH ligands in an acidic environment.

Energy Transfer Occurs from the QD to the J2 Aggregate. The PL of QDs within the conjugates is quenched by the J-agg. In Figure 2C, the PL of the QDs from the QD-1 sample decreases by 97% upon addition of 20 equiv of Cy^+ at pH 7.7. Under these conditions, 70% of Cy^+ molecules are part

DOI: 10.1021/jacs.6b04087
J. Am. Chem. Soc. 2016, 138, 9557−9564

of J2-type aggregates, which absorb at approximately the same set of wavelengths that the QDs emit (see Figure 2B). Moreover, for this sample, a sharp fluorescence peak from J2 appears at 1047 nm on the top of QD emission background upon nearly selective excitation of the QDs at 470 nm (a local minimum of dye absorption). This sharp feature matches that of the J2 emission upon direct excitation of J2 at 980 nm (Figure 2C, inset). The observation of fluorescence from J2 upon excitation of the QDs indicates that efficient excitonic EnT from the QDs to J2 is occurring, especially because the intrinsic fluorescence quantum yield of the J-agg formed by IR140 (either Cy^+ or Cy^-) is very low. We have measured the fluorescence quantum yield of the J-aggregate formed by IR140-Cy^-, which has similar absorption spectrum to J2, 0.2%. By comparing the J2 emission from direct excitation (at 980 nm) to that from QD exciton injection, and considering the relative absorbances of the QD and J2 at those wavelengths, we estimate an EnT quantum yield for the QD/J2 system of 83−100% (see Figure S2).

Adding the same amount of Cy^+ dye to the QD-3 sample at pH 5.7 results a conjugate with 100% of Cy^+ molecules in the J1-agg form and 20% less total dye loading than for the QD-1/J2 system. In these QD/J1 conjugates, the QD PL decreases by 85%, and the remaining PL spectrum of the QD is shifted slightly to higher energy than that of the QDs alone, probably due to etching of the QDs in a weakly acidic environment (Figure S3). We observe no J1 emission from the QD/J1 conjugate on top of the QD PL background, upon either excitation of the QD or direct excitation of J1 at 930 nm. The J1-type aggregate has a less-ordered structure than J2. Thus, unlike J2, its radiative relaxation rate is not enhanced through coherent coupling of constituent transition dipoles,[29] and the fluorescence in J1 does not compete as favorably with fast nonradiative processes as in J2.

Energy Transfer within the QD/J2 Conjugate Occurs in Less than 1 ns. The dynamics of the J-agg and QD excited states provide further evidence that EnT occurs efficiently within the QD/J2 aggregate due to excellent spectral overlap of donor and acceptor and that EnT occurs much less efficiently within the QD/J1 conjugate due to poor overlap of donor and acceptor. We monitor the dynamics of the EnT process with transient absorption (TA) measurements on the picosecond time scale in the NIR spectral window (850−200 nm, Figure 3A). The NIR TA spectra of the QD-1/J-aggregate sample, which is 70% QD/J2 and 30% QD/J1 so we refer to it as "QD/J2", are dominated by the signal from J2, which consists of a large ground-state bleach at 1040 nm and a photoinduced absorption band between ∼950 and 1000 nm. The ground-state bleach of the QD bandgap transition (at ∼900 nm) is also distinguishable from the J2 signal (see the 10 ps trace in Figure 3A). The ground-state absorption spectrum of this sample suggests the existence of J1, but in the TA spectra, the J1 signal is overwhelmed by the J2 signal, probably because the transition dipole moment (and therefore the ground-state depletion) of an exciton-coupled system depends on the number of coherently coupled (N_{coh}) molecules in the excitonic state, which is much higher for the ordered J2 than the disordered J1 (see the Supporting Information for our estimates of N_{coh}).[29]

We monitor the intrinsic exciton relaxation dynamics of the J2-aggregate by pumping J2 directly at 980 nm (Figure 3B, black). The Supporting Information contains these fits and fit parameters. Kinetics in these aggregates are very complicated because of the involvement of exciton migration and annihilation processes,[42,43] but using previous reports, we can tentatively assign two fast components (0.34 and 2.25 ps) to annihilation of many-exciton and biexciton states through excited state annihilation,[29,43] a 20 ps component to biexciton annihilation among different mesoaggregates through a long-range dipolar interaction,[44] and a 450 ps component to decay of the single exciton via radiative or nonradiative process, such as intersystem crossing.[45] The early kinetics of the bleach may be also affected by the stimulated emission from J2. There are also triplet excited state species observable in this trace, with a lifetime >3 ns.

When QD/J2 is excited at 470 nm (Figure 3B, red), the dynamics of the J2 bleach are markedly different than those when it was excited directly at 980 nm. Specifically, the slower recovery of the bleach at early times (<100 ps) implies a concomitant growth that competes with the intrinsic decay. This growth is better illustrated by plotting the difference between kinetic traces acquired with 470 and 980 nm pumps (Figure 3B, blue). A fit of this difference trace yields two growth processes for the J2 bleach, with time constants of 18 ps (12%) and 340 ps (62%). Comparison of transient absorption spectra acquired with a visible probe to the spectra of chemically oxidized and reduced Cy^+ confirms that both growth components of the bleach of J2 upon excitation of the QD are due to EnT, not charge transfer (see Figure S8 and S9). The growth that occurs in <1 ps is artifactual: specifically, it is due to a slight discrepancy in the IRFs of the two experiments.

The difference trace in Figure 3B only partly deconvolutes the growth and decay processes of the J2 excited state, so 18 and 340 ps are only estimates of the EnT time constants. This deconvolution is complicated by the follwing: (i) coherent coupling of transition dipoles in the J-aggregate could exaggerate the change in bleach amplitude caused by injected excitons from the QD and (ii) the relaxation rates of excitons in J-agg depend on their density, which differs for the scenarios of direct excitation versus EnT from the QD. Despite this complexity, we can conclude that there are at least two EnT pathways with different rates in QD/J2 conjugates and that a large portion of the EnT processes occur with time constants of several hundreds of picoseconds.

We obtain a better estimate for the EnT time constant in the QD/J2 system by monitoring the recovery of the QD ground-state bleach at 880 nm (where interference from the J2 bleach is minimized) after photoexcitation at 470 nm (Figure 4). With no added Cy^+, 14% of the QD bleach recovers with a time constant of 10 ps (due to Auger recombination of biexcitons formed at our pump fluence),[13] but more than 70% of the excited state remains after 3 ns. In contrast, for QD/J2 conjugates, the QD bleach completely recovers within 3 ns, and the kinetic trace can be fitted with three exponential decay terms, as listed in Table 1. In addition to a fast Auger recombination term, there are two slower decay terms with time constants of 90 ps (12%) and 800 ps (75%). The yield of EnT in the QD/J2 system is close to unity (as described above), so we attribute both of the latter two decay components to EnT from the QD to J2. The time constants of these two components do not match those observed for J2 bleach (18 and 340 ps) due to the difficulty in deconvoluting the J2 bleach kinetics, as described in the last paragraph. Because the kinetic trace at 880 nm has nearly 100% contribution from the QD, the true EnT time constants for the QD/J2 system are probably closer to the 90 ps/800 ps

DOI: 10.1021/jacs.6b04087
J. Am. Chem. Soc. 2016, 138, 9557−9564

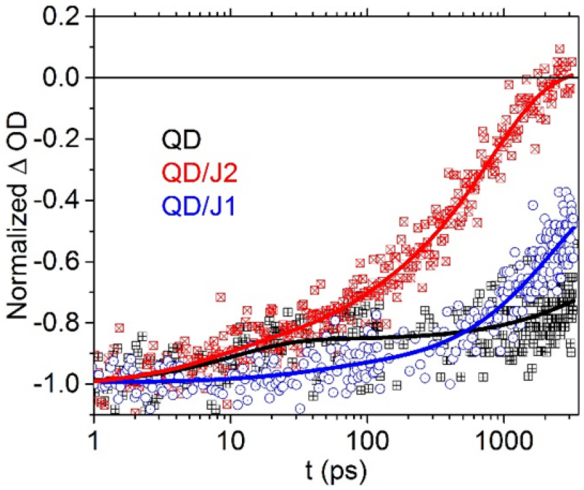

Figure 4. Kinetic traces of the recovery of the ground-state bleach of the QD-only sample (black) and of the conjugates QD/J2 (red) and QD/J1 (blue), all monitored at 880 nm after 470 nm excitation. We choose to monitor the high-energy side of QD ground-state bleach to minimize interference from the overlapping photoinduced absorption signals from the J-agg. The decay traces are fit with a sum of exponential functions with parameters listed in Table 1.

measured at 880 nm than to the 18 ps/340 ps measured at 1040 nm.

We also monitored the dynamics of the QD/J1 conjugates upon photo excitation of either the J1 aggregate (with a 930 nm pump) or the QDs (with a 470 nm pump, Figure 3C,D). The difference in dynamics of J1 acquired with these two pump wavelengths, plotted in blue in Figure 3D, is very small, but can be fit with two exponential terms with time constants of 6 and 1200 ps (Table 1). We assign the 1200 ps component to EnT from the QD to J1 because it is closest to the EnT time constant we obtain by fitting the dynamics of the ground-state bleach of the QD at 880 nm; the bleach of the QD recovers with an additional time constant of 2.2 ns in the presence of the J1 aggregate. It is possible that the 6 ps time constant corresponds to charge transfer from the QD to J1; however, the relative energy levels of the QD and J1 makes charge transfer even less likely in this conjugate than in QD/J2. No kinetic term with a similar time constant is observed for the decay of the QD bleach, so we believe that this component is an artifact of the subtraction procedure, mostly due to the difficulty in replicating exactly the excitation conditions for J1 in the 470 nm pumped and 930 nm pumped experiments.

The comparison of the dominant EnT rate constants for QD/J2 ($\leq$(800 ps)$^{-1}$) and QD/J1 ($\leq$(2.2 ns)$^{-1}$) conjugates suggests that EnT occurs through a Förster (FRET) mechanism, for which the rate constant is proportional to spectral overlap between the donor emission and the acceptor absorption:

$$k_{DA} = \frac{1}{\tau_R}\frac{1}{d^6}\frac{9\kappa^2}{128\pi^5 n^4}\int \lambda^4 F_D(\lambda)\,\sigma_A(\lambda)\,d\lambda \quad (1)$$

where τ_R is the intrinsic radiative lifetime of the donor, d is the distance betweenthe centers of the transition dipoles of donor and acceptor, κ is a measure of the relative orientation of the transition dipoles, n is the refractive index of the surroundings, and the integral quantifies the spectral overlap between the donor emission and the acceptor absorption. If we assume that all quantities except for spectral overlap are similar for QD/J1 and QD/J2, then strictly on the basis of the differences in spectral overlap for the two conjugates and accounting for the different dye loadings and J1/J2 ratios in the two cases, eq 1 predicts that the rate constant for FRET should be approximately a factor of 3 larger for the QD/J2 conjugate than for the QD/J1 conjugate (see the Supporting Information for the detailed calculation). This prediction closely agrees with the FRET rate constants extracted from fits of the recovery of the QD ground-state bleach (Figure 4, (800 ps)$^{-1}$ for QD/J2 and (2200 ps)$^{-1}$ for QD/J1).

In QD/J2, the subnanosecond EnT lifetime is a factor of 10−100 shorter than lifetimes observed for systems where the PbS QD is both the energy donor and energy acceptor, which are typically tens to hundreds of nanoseconds.[20−23] Although the FRET rate in our system is still limited by the long radiative lifetime of the PbS QD donor (2−3 μs),[21] we believe that we achieve a fast FRET process because (i) the oscillator strength (per cyanine dye molecule) of the S_1 transition of the J-agg is approximately a factor of 3 larger than that of the first excitonic absorption of a PbS QD with a bandgap absorption at the same wavelength (1040 nm), (ii) the narrow absorption profile of J2 concentrates the oscillator strength of the acceptor to achieve optimal spectral overlap with the QD emission, (iii) the formation of large J-agg on the surface of QD ensures that each donor is surrounded by a large number of acceptors, such that the FRET rate is statistically enhanced by multiple possible

Table 1. Multiexponential Fitting Parameters for Dynamics within Photoexcited PbS QD/J-aggregate Conjugates

system	$\lambda_{pump}/\lambda_{probe}$ (nm) (pumped species/probed species)	τ_1 (ps) (amp., %) unassigned[b]	τ_2 (ps) (amp., %) Auger recomb.[b]	τ_3 (ps) (amp., %) EnT 1[b]	τ_4 (ps) (amp., %) EnT 2[b]	τ_5 (ps) (amp., %) exciton decay[b]
QD[a]	470/880		10 ± 4			>3000
	(QD/QD)		(−14 ± 2)			(−86 ± 5)
QD/J2	470/880		10[c]	90 ± 60	800 ± 100	
	(QD/QD)		(−13 ± 3)	(−12 ± 4)	(−75 ± 4)	
QD/J1	470/880		10[c]	2200 ± 300		>3000
	(QD/QD)		(−5 ± 2)	(−61 ± 4)		(−34 ± 5)
QD/J2	470/1040 − 980/1040			18 ± 2	340 ± 20	>3000
	(QD/J2 − J2/J2)			(16 ± 2)	(84 ± 4)	(−100 ± 30)
QD/J1	470/965 − 930/965	6 ± 1		1200 ± 300		>3000
	(QD/J1 − J1/J1)	(73 ± 7)		(27 ± 20)		(−100 ± 10)

[a]The values listed are for QD-1; QD-3 has almost identical dynamics (see Figure S6). [b]For bleach signals, positive amplitudes represent growths and negative amplitudes represent recoveries. [c]The time constant was fixed to the Auger recombination time constant for the QD-only sample in order to constrain the fit.

DOI: 10.1021/jacs.6b04087
J. Am. Chem. Soc. 2016, 138, 9557−9564

FRET pathways (the acceptor/donor ratio is >10:1 for QD versus J2 in terms of Cy^+ molecules), and (iv) the J-agg can be considered to be a "bulky" exciton acceptor, such that the sixth-order dependence of the FRET rate on donor−acceptor distance is reduced to a third-order dependence.[46] These properties of QD/J-agg conjugates have led to even faster FRET ($k_{DA} \geq (50\ ps)^{-1}$)[17,18] for visible-wavelength excitons using shorter-lifetime cadmium chalcogenide QDs as energy donors.

Finally, the multiple time constants we observe for FRET in the PbS QD/J-agg conjugates may be related to a distribution of relative orientations and distances between the transition dipoles of the QD donors and J-agg acceptors. We used a value of $^2/_3$ for the orientation factor κ^2 in eq 1[19,47,48] because the transition dipole in a symmetrically shaped QD is isotropically aligned.[49,50] A cyanine J-agg, however, includes a set of transition dipoles arranged helically.[30,51] While isotropy of the QD's transition moment ensures that a component of it is always aligned with that of the J-agg, it is also unlikely, given the large possible distribution of J-agg adsorption geometries, that κ^2 achieves its maximum value of 4. We will therefore always observe a distribution of FRET rates. Multiple FRET pathways with different rates have also been reported in a system consist of CdTe QDs and cyanine J-agg.[16] The most straightforward way to maximize the FRET rate via transition dipole alignment is to (i) control the adsorption geometry of the J-aggregate precisely and (ii) use a nonspherical QD with a well-defined transition dipole moment orientation. Employing oriented transition dipoles has resulted in large increases in FRET rates among, for instance, CdSe nanoplatelet donors and acceptors.[15]

CONCLUSIONS

We prepared aqueous dispersions of electrostatically assembled conjugates of PbS QDs and J-agg of a cyanine dye, IR140-Cy^+. By controlling the surface coverage of the negatively charged glutathione ligands on the surface of the QDs and the pH of the solution, we controlled the structure and optical spectra of adsorbed J-agg. We observe subnanosecond resonance EnT of near-infrared excitons from the PbS QDs to the J-agg by maximizing the spectral overlap of donor and acceptor.

For our optimal system, a majority of EnT occurs within 800 ps, which is much faster than the recently reported Dexter-type EnT from PbS(Se) QDs to the triplet excited state of rubrene. The fastest component of EnT that we observe has a time constant of 90 ps and is therefore competitive with the Auger recombination of the biexcitonic state in PbS QDs, which has a lifetime between 10 and 200 ps (depending on the particle dimensions).[13,26,27] Though we do not have evidence that EnT in our QD/J-agg conjugates is directly competing with the Auger recombination, the decoration of PbS QDs with molecular J-agg of the appropriate structure and coverage is a promising strategy for extracting one or both excitons from a biexciton in a lead chalcogenide QD. If this biexciton is created from a higher-energy exciton through a carrier multiplication process,[9,10] then QD/J-agg conjugates (in particular, those with anisotropically shaped QDs and controlled J-agg adsorption geometries) should be efficient visible-to-NIR downconverters.

ASSOCIATED CONTENT

Supporting Information

The Supporting Information is available free of charge on the ACS Publications website at DOI: 10.1021/jacs.6b04087.

Molecular structures; solubility of the cyanine dyes; estimation of EnT quantum yield; steady-state PL of QD/J1; Calculation of the number of coherence; QD kinetics; kinetic fits for J-agg; visible TA and absorption spectra of chemical reduction/oxcdization products of QD/J; estimation of FRET rate ratio (PDF)

AUTHOR INFORMATION

Corresponding Author

*e-weiss@northwestern.edu

Notes

The authors declare no competing financial interest.

ACKNOWLEDGMENTS

This material is based on upon work supported by the Air Force Office of Scientific Research, under AFOSR award No. FA-9550-14-1-0005.

REFERENCES

(1) Kramer, I. J.; Levina, L.; Debnath, R.; Zhitomirsky, D.; Sargent, E. H. *Nano Lett.* **2011**, *11*, 3701−3706.
(2) Luther, J. M.; Law, M.; Beard, M. C.; Song, Q.; Reese, M. O.; Ellingson, R. J.; Nozik, A. J. *Nano Lett.* **2008**, *8*, 3488−3492.
(3) Zhao, N.; Osedach, T. P.; Chang, L.-Y.; Geyer, S. M.; Wanger, D.; Binda, M. T.; Arango, A. C.; Bawendi, M. G.; Bulovic, V. *ACS Nano* **2010**, *4*, 3743−3752.
(4) Wang, C.; Thompson, R. L.; Ohodnicki, P.; Baltrus, J.; Matranga, C. *J. Mater. Chem.* **2011**, *21*, 13452−13457.
(5) Ratanatawanate, C.; Tao, Y.; Balkus, K. J. *J. Phys. Chem. C* **2009**, *113*, 10755−10760.
(6) Li, L.; Dai, H.; Feng, L.; Luo, D.; Wang, S.; Sun, X. *Nanoscale Res. Lett.* **2015**, *10*, 418.
(7) Michalet, X.; Pinaud, F. F.; Bentolila, L. A.; Tsay, J. M.; Doose, S.; Li, J. J.; Sundaresan, G.; Wu, A. M.; Gambhir, S. S.; Weiss, S. *Science* **2005**, *307*, 538−544.
(8) Deng, D.; Xia, J.; Cao, J.; Qu, L.; Tian, J.; Qian, Z.; Gu, Y.; Gu, Z. *J. Colloid Interface Sci.* **2012**, *367*, 234−240.
(9) Schaller, R. D.; Klimov, V. I. *Phys. Rev. Lett.* **2004**, *92*, 186601.
(10) Ellingson, R. J.; Beard, M. C.; Johnson, J. C.; Yu, P.; Micic, O. I.; Nozik, A. J.; Shabaev, A.; Efros, A. L. *Nano Lett.* **2005**, *5*, 865−871.
(11) Nozik, A. J. *Phys. E* **2002**, *14*, 115−120.
(12) Hanna, M. C.; Nozik, A. J. *J. Appl. Phys.* **2006**, *100*, 074510.
(13) Smith, C.; Binks, D. *Nanomaterials* **2014**, *4*, 19−45.
(14) Klimov, V. I. *Annu. Rev. Condens. Matter Phys.* **2014**, *5*, 285−316.
(15) Rowland, C. E.; Fedin, I.; Zhang, H.; Gray, S. K.; Govorov, A. O.; Talapin, D. V.; Schaller, R. D. *Nat. Mater.* **2015**, *14*, 484−489.
(16) Savateeva, D.; Melnikau, D.; Lesnyak, V.; Gaponik, N.; Rakovich, Y. P. *J. Mater. Chem.* **2012**, *22*, 10816−10820.
(17) Halpert, J. E.; Tischler, J. R.; Nair, G.; Walker, B. J.; Liu, W.; Bulovic, V.; Bawendi, M. G. *J. Phys. Chem. C* **2009**, *113*, 9986−9992.
(18) Zhang, Q.; Atay, T.; Tischler, J. R.; Bradley, M. S.; Bulovic, V.; Nurmikko, A. V. *Nat. Nanotechnol.* **2007**, *2*, 555−559.
(19) Achermann, M.; Petruska, M. A.; Crooker, S. A.; Klimov, V. I. *J. Phys. Chem. B* **2003**, *107*, 13782−13787.
(20) Xu, F.; Ma, X.; Haughn, C. R.; Benavides, J.; Doty, M. F.; Cloutier, S. G. *ACS Nano* **2011**, *5*, 9950−9957.
(21) Clark, S. W.; Harbold, J. M.; Wise, F. W. *J. Phys. Chem. C* **2007**, *111*, 7302−7305.
(22) Corricelli, M.; Enrichi, F.; Altamura, D.; De Caro, L.; Giannini, C.; Falqui, A.; Agostiano, A.; Curri, M. L.; Striccoli, M. *J. Phys. Chem. C* **2012**, *116*, 6143−6152.
(23) Litvin, A. P.; Ushakova, E. V.; Parfenov, P. S.; Fedorov, A. V.; Baranov, A. V. *J. Phys. Chem. C* **2014**, *118*, 6531−6535.
(24) Huang, X.; Xu, Q.; Zhang, C.; Wang, X.; Xiao, M. *Nano Lett.* **2016**, *16*, 2492−2496.

DOI: 10.1021/jacs.6b04087
J. Am. Chem. Soc. 2016, 138, 9557−9564

(25) Huang, Z.; Simpson, D. E.; Mahboub, M.; Li, X.; Tang, M. L. *Chem. Sci.* **2016**, *7*, 4101−4104.
(26) Robel, I.; Gresback, R.; Kortshagen, U.; Schaller, R. D.; Klimov, V. I. *Phys. Rev. Lett.* **2009**, *102*, 177404.
(27) Padilha, L. A.; Stewart, J. T.; Sandberg, R. L.; Bae, W. K.; Koh, W. K.; Pietryga, J. M.; Klimov, V. I. *Acc. Chem. Res.* **2013**, *46*, 1261−1269.
(28) Kasha, M. *Radiat. Res.* **1963**, *20*, 55−70.
(29) Knoester, J.; Spano, F. C. In *J-aggregates*; Kobayashi, T., Ed.; World Scientific Publishing Co.: Singapore, 1996; pp 111−160.
(30) Würthner, F.; Kaiser, T. E.; Saha-Möller, C. R. *Angew. Chem., Int. Ed.* **2011**, *50*, 3376−3410.
(31) Hines, M. A.; Scholes, G. D. *Adv. Mater.* **2003**, *15*, 1844−1849.
(32) McArthur, E. A.; Morris-Cohen, A. J.; Knowles, K. E.; Weiss, E. A. *J. Phys. Chem. B* **2010**, *114*, 14514−14520.
(33) Algar, W. R.; Krull, U. J. *ChemPhysChem* **2007**, *8*, 561−568.
(34) Giansante, C.; Carbone, L.; Giannini, C.; Altamura, D.; Ameer, Z.; Maruccio, G.; Loiudice, A.; Belviso, M. R.; Cozzoli, P. D.; Rizzo, A.; Gigli, G. *J. Phys. Chem. C* **2013**, *117*, 13305−13317.
(35) Giansante, C.; Infante, I.; Fabiano, E.; Grisorio, R.; Suranna, G. P.; Gigli, G. *J. Am. Chem. Soc.* **2015**, *137*, 1875−1886.
(36) Mohanty, J.; Palit, D. K.; Mittal, J. P. *PINSA-A: Proc. Indian Natl. Sci. Acad., Part A* **2000**, *66*, 303−315.
(37) Berlepsch, H. v.; Böttcher, C. *J. Photochem. Photobiol., A* **2010**, *214*, 16−21.
(38) Ferretti, L.; Elviri, L.; Pellinghelli, M. A.; Predieri, G.; Tegoni, M. *J. Inorg. Biochem.* **2007**, *101*, 1442−1456.
(39) Hyun, B.-R.; Zhong, Y.-W.; Bartnik, A. C.; Sun, L.; Abruña, H. D.; Wise, F. W.; Goodreau, J. D.; Matthews, J. R.; Leslie, T. M.; Borrelli, N. F. *ACS Nano* **2008**, *2*, 2206−2212.
(40) Lenhard, J. R.; Hein, B. R. *J. Phys. Chem.* **1996**, *100*, 17287−17296.
(41) Billsten, H. H.; Sundstrom, V.; Polivka, T. *J. Phys. Chem. A* **2005**, *109*, 1521−1529.
(42) Gretchikhine, A.; Schweitzer, G.; Van der Auweraer, M.; De Keyzer, R.; Vandenbroucke, D.; De Schryver, F. C. *J. Appl. Phys.* **1999**, *85*, 1283−1293.
(43) Völker, S. F.; Schmiedel, A.; Holzapfel, M.; Renziehausen, K.; Engel, V.; Lambert, C. *J. Phys. Chem. C* **2014**, *118*, 17467−17482.
(44) Sundström, V.; Gillbro, T.; Gadonas, R. A.; Piskarskas, A. *J. Chem. Phys.* **1988**, *89*, 2754−2762.
(45) McRae, E. G.; Kasha, M. *J. Chem. Phys.* **1958**, *28*, 721−722.
(46) Rogach, A. L.; Klar, T. A.; Lupton, J. M.; Meijerink, A.; Feldmann, J. *J. Mater. Chem.* **2009**, *19*, 1208−1221.
(47) Crooker, S. A.; Hollingsworth, J. A.; Tretiak, S.; Klimov, V. I. *Phys. Rev. Lett.* **2002**, *89*, 186802.
(48) Mork, A. J.; Weidman, M. C.; Prins, F.; Tisdale, W. A. *J. Phys. Chem. C* **2014**, *118*, 13920−13928.
(49) Htoon, H.; Furis, M.; Crooker, S. A.; Jeong, S.; Klimov, V. I. *Phys. Rev. B: Condens. Matter Mater. Phys.* **2008**, *77*, 035328.
(50) Tice, D. B.; Weinberg, D. J.; Mathew, N.; Chang, R. P. H.; Weiss, E. A. *J. Phys. Chem. C* **2013**, *117*, 13289−13296.
(51) Megow, J.; Rohr, M. I. S.; Schmidt am Busch, M.; Renger, T.; Mitric, R.; Kirstein, S.; Rabe, J. P.; May, V. *Phys. Chem. Chem. Phys.* **2015**, *17*, 6741−6747.

DOI: 10.1021/jacs.6b04087
J. Am. Chem. Soc. 2016, 138, 9557−9564